An Electrochemically Initiated Self-Limiting Hydrogel Electrolyte for Dendrite-Free Zinc Anode

Yuetao Wang, Luyi Yang, Pengfei Xu, Lele Liu, Shunning Li, Yan Zhao,* Runzhi Qin,* and Feng Pan*

The zinc dendrite growth generally relies upon a "positive-feedback" mode, where the fast-grown tips receive higher current densities and ion fluxes. In this study, a self-limiting polyacrylamide (PAM) hydrogel that presents negative feedback to dendrite growth is developed. The monomers are purposefully polymerized at the dendrite tips, then the hydrogel reduces the local current density and ion flux by limiting zinc ion diffusion with abundant functional groups. As a consequence, the accumulation at the dendrite tips is restricted, and the (002) facets-oriented deposition is achieved. Moreover, the refined porous structure of the gel enhances Coulombic Efficiency by reducing water activity. Due to the synergistic effects, the zinc anodes perform an ultralong lifetime of 5100 h at 0.5 mA cm^{-2} and 1500 h at 5 mA cm^{-2}, which are among the best records for PAM-based gel electrolytes. Further, the hydrogel significantly prolongs the lifespan of zinc-ion batteries and capacitors by dozens of times. The developed in situ hydrogel presents a feasible and cost-effective way to commercialize zinc anodes and provides inspiration for future research on dendrite suppression using the negative-feedback mechanism.
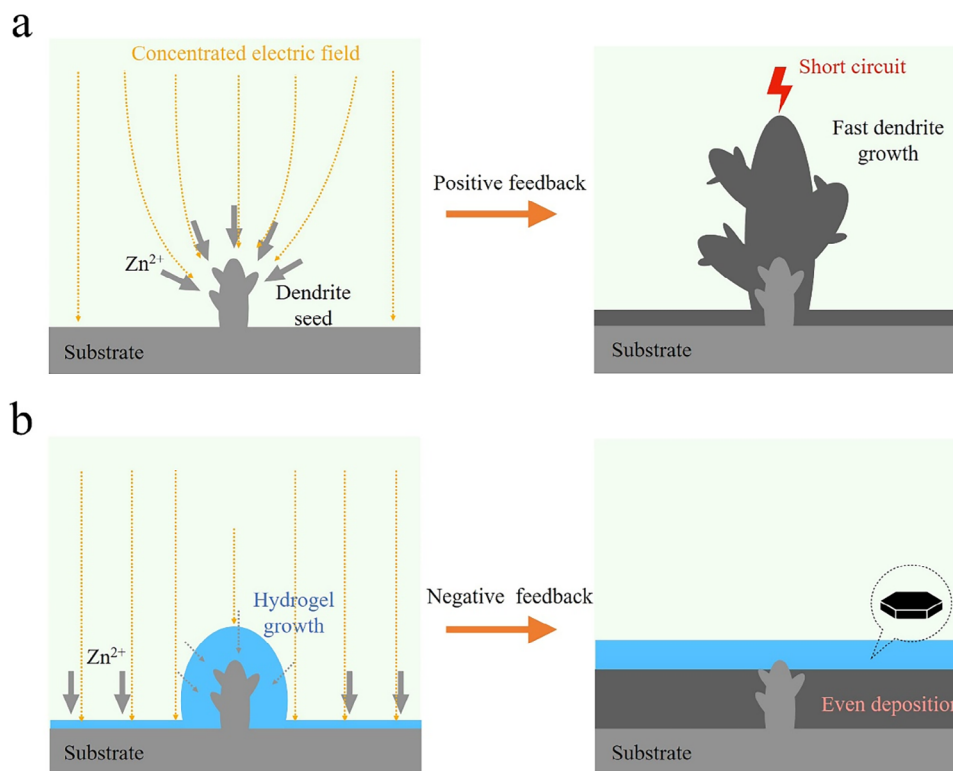
1. Introduction

Aqueous zinc-ion batteries (ZIBs) have been regarded as promising candidates for large-scale energy storage devices due to their high safety, economic viability, and high capacity.[1] It should be noted that these superiorities mainly stem from zinc metal anodes. On one hand, zinc metal presents the lowest potential among the practicable metals in aqueous electrolytes (-0.76 V$_{SHE}$) and a relatively large capacity (820 mAh g^{-1} and 5855 mAh cm^{-3}), guaranteeing the energy density and power density of the full cell.[2] On the other hand, it is abundant in resources and has a mature production process, offering a very low cost (≈ 2 USD kg^{-1}) for price-sensitive applications.[3] However, the zinc anode suffers from poor electrochemical performance, including short cycling lifetimes that originate from arbitrary dendrite formation,[4,5] and low reversibility relating to the high activity of water molecules.[6] Traditionally, the zinc anode can only cycle for a few dozen hours, which is far from satisfactory.[7]

The dendrite formation is thermodynamically favorable for zinc anode and other metallic anodes,[8–10] which bothers the scientific fields for dozens of years. The difficulty for morphology control lies in the fact that the dendrite growth follows the positive feedback mode without confinement. Certain dendrite seeds with faster deposition rates become prominent in shape and receive more concentrated electric fields and ion flux locally. In turn, these intensified current densities and ion flux contributes to an even higher local deposition rate (**Figure 1**a). As a result, the dendrite tips grow much faster than other planar sites, which is known as the "tip effect", being an intrinsic property for metallic anodes. For example, it has been reported that zinc anodes with defects and rough surfaces are more vulnerable to short circuits in batteries.[5]

So far, continuous efforts have been made to address these dendritic issues and to enhance the performance of ZIBs. Most if not all of the literature focus on weakening the positive feedback of the dendrites. For example, the surface coatings are employed to decrease the local concentration of the electric field and redistribute the diffusion of zinc ions due to the sieve effect.[11,12] Besides, electrolyte tuning is considered as an effective way, for it can change the chemical environment of the zinc ions and make guidance for their diffusion. It is recognized the zinc ions can be coordinated by the foreign solvents with functional groups,[13] then regularly arranged functional groups can provide consecutive diffusion pathways to counterwork the tendency of the positive feedback.[14,15] However, such strategies are designed for working homogeneously and statically. Once applied, they are unable to distinguish the dendrite sites among the planar depositions, thus being out of depth to handle the dynamic morphology variation, especially for the large-size defects.

Herein, we propose an electrochemically initiated hydrogel that alters the zinc deposition mode from positive feedback to a negative one. The current-sensitive hydrogel grows faster at dendrite sites with higher electric fields, then hinders the arbitrary

Y. Wang, L. Yang, P. Xu, L. Liu, S. Li, Y. Zhao, R. Qin, F. Pan
School of advanced materials
Peking University Shenzhen Graduate School
Shenzhen 518055, China
E-mail: zhaoyan@pku.edu.cn; bushihaoren@pku.edu.cn; panfeng@pkusz.edu.cn

Figure 1. Schematic diagram of zinc dendrite evolution in a) traditional electrolyte with positive feedback and b) in situ gel electrolyte with negative feedback.

growth by controlling the ion diffusion (Figure 1b). This hydrogel electrolyte is self-adaptive for dendrite suppression and capable of fitting to extreme configurations, even with a large curvature radius of realistic metal electrodes. Additionally, the refined 3D structure in the hydrogel aids in oriented zinc deposition and enhances the confinement of free water, contributing to the ultra-stability of the zinc anode. The in situ hydrogel can cycle for >5100 h without evidence of decay, outperforming traditional electrolytes and ex situ gels. Moreover, the hydrogel can also be applied to full batteries with various cathode materials, highlighting its high practical value. This novel gelation process has the potential to advance future research on zinc-based energy storage devices.

2. Results and Discussion

2.1. Electrochemically Induced In Situ Gelation Process

Most if not all of the literature focus on weakening the positive feedback of the dendrites. The goal of dynamic morphology control could only be achieved by the dynamic manipulation of the electrode reactions, which is inaccessible to the traditional static strategies mentioned above. Here we propose an electrochemically induced polyacrylamide (PAM) hydrogel electrolyte. In the precursor solution that consists of monomer (acrylamide, AM) and cross-linking agent (N, N′-methylene bisacrylamide, MBAA). The galvanostatic protocol of 5 mA cm^{-2} and 2.5 mAh cm^{-2} is applied to trigger the electrochemical cross-link onto the electrode surface. As visualized in the in situ optical microscope images in

Figure 2a, the liquid electrolyte turns to appear blurry and less lustrous. The magnified image exhibits a clear fiber-like configuration, which is attributed to the birefringence, a typical characteristic of anisotropic hydrogels.[16] Then a piece of colorless and transparent hydrogel can be distinguished (Figure 2b). Notably, the gel completely wraps the electrode without exfoliation, indicating strong adhesion (Figure 2c). The zinc/hydrogel composite electrode is thus prepared in a single step. It is worth noting that such in situ gel process is related to the temperature, and it cannot be realized at low temperatures (≈0 °C).

The gelation process is further recorded by in situ Raman spectra shown in Figure 2d. The precursor solution displays strong peaks at 1443, 1635, 3040, and 3116 cm^{-1}, which can be assigned to CH$_2$ bending, C=C stretching, vinyl C—H, and vinyl CH$_2$ asymmetric stretching of AM and MBAA.[17] This profile is similar to that of the AM monomer (Figure S1, Supporting Information). During electrolysis, the peak at 3040 cm^{-1} decays while the one at 2932 cm^{-1} increases within ≈5 min, indicating the breakage of C=C bonds and the emergence of C—C bonds, respectively. The rapid formation of the hydrogel is also testified by the energy dipersive spectroscopy (EDS) mapping of the zinc surface. As shown in Figure S2 (Supporting Information), the homogenous distribution of N element indicates the successful formation of amide-contained hydrogel within 3 min. After 0.5 h, the C=C bond signal disappears, and the C—C bond signal dominates, indicating the complete transformation from AM monomer to PAM hydrogel. Moreover, an ex situ PAM hydrogel is also prepared using ammonium persulfate (APS) as the initiator, which quickly gels in 5 min with heat release, forming a

ADVANCED
SCIENCE NEWS

www.advancedsciencenews.com

NANO · MICRO
small

www.small-journal.com
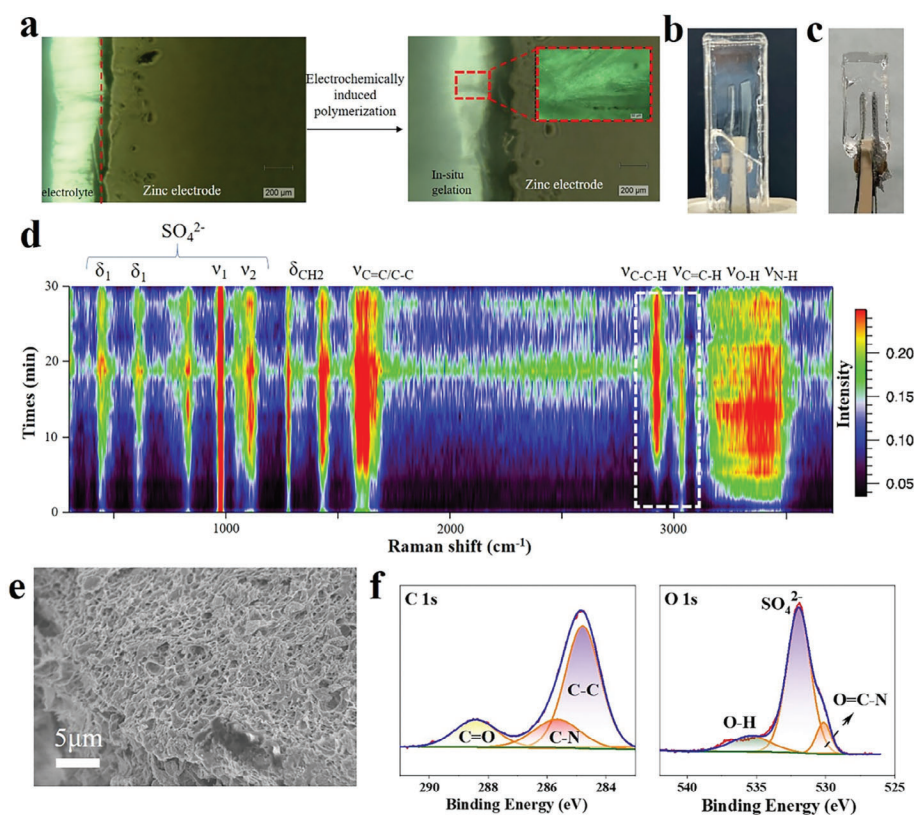
Figure 2. a) Optical photos of the gelation process; b,c) optical photos of the hydrogel; d) in situ Raman spectra of the gelation process; e) SEM image of the hydrogel; f) XPS spectra of C1s and O1s of the hydrogel.

piece of rubber-like transparent gel (Figure S3, Supporting Information) with similar Raman peaks at 2932 cm^{-1} (Figure S4, Supporting Information). In addition, both the gels show similar mechanical properties (Figure S5, Supporting Information). Therefore, it can be inferred that the initiator-free hydrogel generated in situ has no chemical and physical difference from the traditional initiator-used hydrogel.

The microstructure of in situ hydrogel and the traditional ex situ one is shown in Figure 2e and Figure S6 (Supporting Information). Generally, both the two gels have porous structures in their inner regions. The in situ hydrogel has smaller pores with a diameter of ≈0.5 µm compared to the ex situ one, which has a diameter of ≈3 µm. The more refined structure of the in situ gel may be due to the progressive gelation process initiated by electrochemical protocols. As the concentration of monomer is equal in both gels, the refined structure of the in situ gel exposes a larger specific area and more functional groups, which is beneficial to the electrochemical performance as discussed below. Additionally, the EDS mapping of the in situ hydrogel is presented in Figure S7 (Supporting Information). The uniform distribution of C, O, S, N, and Zn elements in the EDS mapping shows that the in situ hydrogel uniformly covers the zinc surface after polymerization. The X-ray photoelectron spectroscopy (XPS) results further verify the chemical states of the elements. No signal of C=C bond is discovered in the C1s spectrum (Figure 2f), indicating the complete exhaustion of the monomer and the successful polymerization. Then the spectra of O1s (Figure 2f), N1s, and S2p

(Figure S8, Supporting Information) prove the other functional groups are not affected by the electrochemical conditions.

One significant difference between the in situ hydrogel and the traditional one is the origination of the gelation process. In traditional cases, the initiator such as ammonium persulfate or 2-Hydroxy-4′ (2-hydroxyethyl)−2-methylpropiophenone is required in the precursor solution to produce primary radicals. These radicals are evenly generated and dispersed in the electrolyte, leading to homogeneous polymerization of monomers at each site in the spatial scale, and almost simultaneously in the time scale. Once initiated, the traditional gelation process cannot stop before the exhaustion of monomers, then the polymers quickly fill in the whole electrolyte randomly and indiscriminately within minutes or hours. This process exhibits slow initiation and fast propagation, typical of a chain reaction. Therefore, the traditional hydrogel is always static with a homogeneous structure and configuration, which fails to handle the morphology evolution of the zinc anode. In contrast, no initiator is added to the precursor solution in our cases. The monomers are electrochemically polymerized, endowing the hydrogel with the capability for stronger dendrite suppression as discussed below.

2.2. Hydrogel with Negative Feedback to Dendrite Development

The in situ gelation process presents a space-dependent and time-dependent character. The gel appears at the very adjacency

**ADVANCED
SCIENCE NEWS**
www.advancedsciencenews.com

NANO · MICRO
small
www.small-journal.com
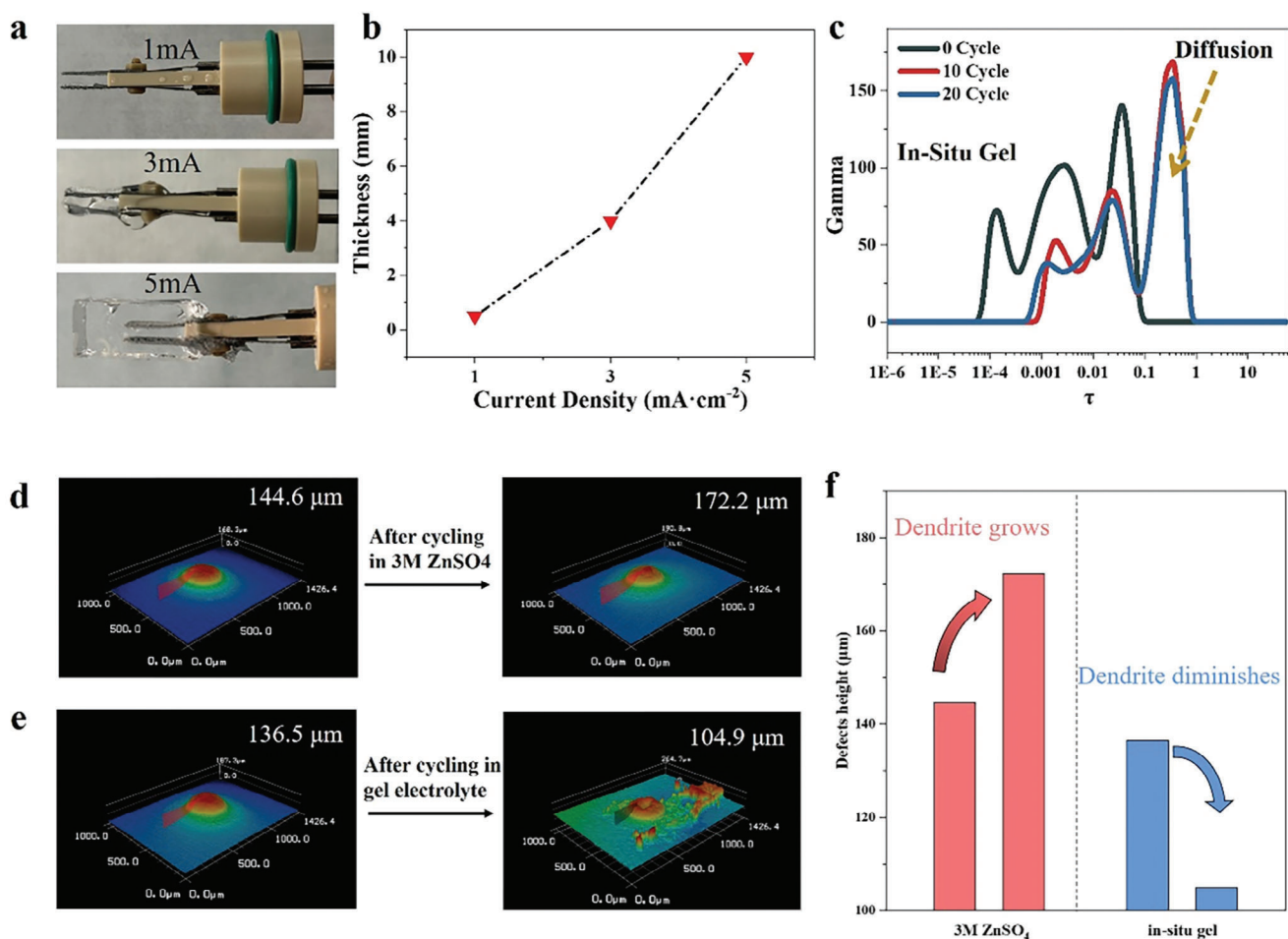
Figure 3. a) Optical photos of the in situ gel variation at different current densities; b) thickness of the in situ gel at different current densities; c) DRT results of zinc electrode in gel electrolytes; CLSM images of the artificial defect evolution in d) 3 M ZnSO₄ electrolyte and e) gel electrolyte; f) height changes of the defects in different electrolytes.

of the zinc electrode instead of the whole electrolyte, then it dynamically grows from the electrode towards the bulk electrolyte, which is the orientation of the electric field (Figure S9, Supporting Information). As a consequence, the gel film covers the zinc surface with a well-bonded interface as the so-called "chemical welding" reported in other literature.[17] More importantly, we find the thickness of the gel is related to the local current density. The thickness variation at different current densities is shown in **Figure 3**a,b. It is clearly observed that higher current density and longer time lead to larger thickness, which can be rationalized as the increased radicals provided from the electrode. Thus, this gelation presents the abnormal character of fast initiation and slow propagation, which provides a precondition for rapid response to local current variations. Then the dynamic hydrogel suppresses dendrite growth with a negative feedback mode.

Generally, the realistic batteries inevitably contain numerous defects, such as roughened surfaces and edges in metal electrodes,[5] and inhomogeneity in electrolytes, which perform as potential dendrite seeds. The attempt to totally eliminate these dendrite seeds does work to some extent, but it is unadvisable considering the economic cost. Once the enhanced zinc plating

is induced at the defects, they further trigger the concentration of the electric field and enhancement of current densities, resulting in dendrite accumulation. In our cases, however, the hydrogel also grows faster at the defects because of higher current densities. With the aid of the refined structure and abundant functional groups, the hydrogel directs the diffusion of zinc ions in a well-organized way, leads to a slightly reduced kinetics of the zinc plating. As a consequence, the dendrite accumulation is hindered. The impedance results shown in Figure S10 (Supporting Information) confirm the confined kinetics of the zinc plating at gel conditions. Further, the analysis of the distribution of relaxation time (DRT) is employed to extract the kinetic information in the impedance results in Figure 3c and Figure S11 (Supporting Information). The timescale issues related to different relaxation times are identified as peaks in the time-domain display, and the ion diffusion is always characterized as the slowest step in the electrochemical reaction.[18,19] Therefore, the strong diffusion peak located at a larger time constant ($\tau = 0.35$ s) in the gel electrolyte gives evidence to slower diffusion process of zinc ions. To the inevitable dendrite seeds, it can be deduced from the nature of the gelation process, the faster the dendrite grows and

the higher the current density conducts, the slower zinc ions diffuse and the heavier the suppression be activated. In this way, the evolution of the hydrogel plays a role in peak shaving and valley filling on the configuration of the zinc surface.

Here we have designed an experiment to clarify the effects of the negative feedback of the in situ hydrogel. A small protrusion is made on a zinc plate using a tweezer tip (Figure S12, Supporting Information). The protrusion has a conical shape with a height of 140 µm and a base radius of 300 µm. Its 3D configuration is recorded using confocal laser scanning microscopy (CLSM), and we believe that it is big enough to simulate common defects. Then galvanostatic stripping and plating are applied to the zinc electrode with the parameters of 5 mA cm^{-2}, 0.83 mAh cm^{-2} and −5 mA cm^{-2}, 2.5 mAh cm^{-2}. Figure S13 (Supporting Information) shows the in situ hydrogel generated on the surface of the zinc plate and the one after peeling from the zinc surface. Compared to the traditional electrolyte (3 M ZnSO$_4$ only), the electrode with in situ hydrogel formation showed slightly higher polarization, which can be rationalized by the energy consumption of the initiation process and the slightly increased diffusion barrier of zinc ions in the hydrogel (Figure S14, Supporting Information). After plating, the defect's height increases by 27.6 µm (from 144.6 to 172.2 µm) in traditional electrolytes, indicating a fast dendrite growth mode (Figure 3d,f). Clearly, the manmade protrusion serves as a lightning rod that attracts the main electric field, making a partial enhancement of zinc deposition. Considering it grows in the scale of tens of micrometers in just 1 cycle, the tip would inevitably evolve to dendrites that leave a short-circuit hazard in the following cycles. In contrast, the defect's height underneath the in situ gel decreases by 31.6 µm (from 136.5 to 104.9 µm), demonstrating the heavily suppressed dendrite evolution (Figure 3e,f). The dynamic protection of the in situ hydrogel limits the diffusion of the zinc ions at the defective site, attenuating the electric field and redistributing the zinc ions. In contrast to other protective coatings that work in a static mode,[17,20–22] the in situ hydrogel shows a self-adaptive behavior never reported before.

It should be noted that the local concentration of the electric field/ion flux reflects the disunity of the electrochemical reaction. Except for the abovementioned defects of the zinc configuration, other nonuniform factors such as ion distribution in the electrolyte,[23] impurity adsorption on the zinc,[24] localized passivation layers on the zinc surface,[25] and chemical differences in crystallographic planes.[4] can also contribute to dendrite formation. These imperfections alter local current densities, leading to positive feedback of current densities and preferential dendrite growth in traditional cases. However, given the current-sensitive nature of the in situ hydrogel, we can reasonably speculate that the in situ gel is capable of providing negative feedback to all sources of imperfection. And such a gelation process may inspire future research on zinc protection.

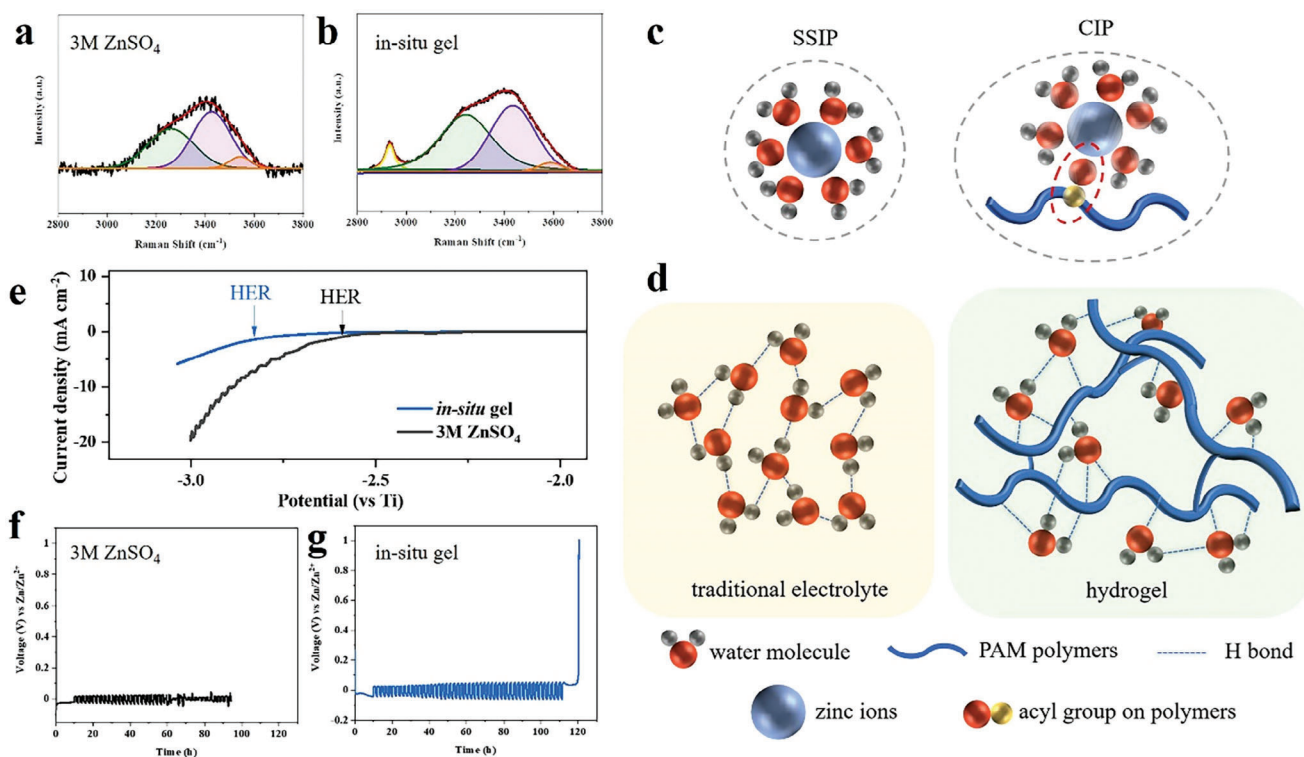### 2.3. Confined Ion Diffusion and Enhanced Efficiency by the Hydrogel

The confined ion diffusion in the hydrogel is achieved by the special structure. **Figure 4**a,b depict a comparison between the Raman profiles of a 3 M ZnSO$_4$ solution and an in situ gel. The broad O─H stretching vibration band can be attributed to three states of water molecules: "network water (NW)" (≈3205 cm^{-1}) for which water molecules form hydrogen bonds with four other molecules, "intermediate water (IW)" (at 3433 cm^{-1}) for which water molecules connect to less than four molecules, and "multimer water (MW)" for which water molecules coordinate with central metal ions.[14] The proportion of each type of water is determined based on the peak area. In contrast to the liquid electrolyte, the in situ gel has a significantly increased NW ratio (from 43.4% to 53.6%) and decreased IW ratio (from 50.6% to 43.4%). These findings suggest that the gel possesses an enhanced hydrogen-bond network, in which more water molecules are bonded with functional groups of the polymer with four hydrogen bonds each. Additionally, the MW ratio in the gel is halved (from 6% to 3%), indicating the traditional hydration shell around the zinc ion is reconstructed. The functional groups of the gel must take part in the coordination considering the hexa-coordination nature of the zinc ions (Figure 4c). This could explain the slightly increased polarization, as the combination of strong electronegativity groups (carbonyl groups) creates higher barriers for the diffusion of zinc ions.

The formation of the hydrogel also enhances the Coulombic efficiency (CE) of the zinc anode. It is well known that zinc's low redox potential of −0.76 V$_{SHE}$ results in high output voltage for the full battery, but may decrease the reaction's reversibility. As shown in Figure 4d, once the hydrogel is formed, more water molecules are bonded in the hydrogen-bond network by the functional groups. Such water molecules are in fact "passivated", possessing a higher energy barrier for hydrogen evolution reaction (HER). The reduced water activity is examined by linear sweep voltammetry technique. Coin-type cells are assembled with titanium and zinc foils as the working and counter electrodes, respectively. A piece of cellulose separator is applied in the cell to simulate the real battery. Since the cellulose material is inert and functionless, it is widely used as the control sample[15] and it shows no impact on the gel performance. Figure 4e shows that the zinc reduction potential is slightly reduced from −2.364 to −2.351 V and the onset HER potential is heavily reduced from −2.594 to −2.785 V under the protection of the in situ hydrogel (current density set to 1 mA cm^{-2}). These results suggest an enlarged HER overpotential from 0.243 to 0.421 V, indicating a strongly depressed HER tendency. The coin-cell was used to measure CE, and Figure 4f,g shows the comparison between the Cu─Zn asymmetrical cell in 3 M ZnSO$_4$ electrolyte and the in situ gel system. The former exhibits low CE and experiences a short circuit after only 30 cycles, indicating the unsatisfactory reversibility of zinc, while the latter shows higher CE in each cycle, with a final CE value of 98.7% within 50 cycles. The superior reversibility enhances the utilization of zinc metal, thereby improving its practicality.

2.4. Electrochemical Performance of Zinc Anode

Coin-type symmetric cells are assembled to evaluate the electrochemical performance of zinc anodes. In the 3 M ZnSO$_4$ electrolyte, the bare zinc electrode was only able to operate safely for 22 h at 0.5 mA cm^{-2} and 0.5 mAh cm^{-2} before a sudden voltage drop at the 11th cycle. The short-circuit failure is authenti-

**ADVANCED
SCIENCE NEWS**

www.advancedsciencenews.com

**NANO · MICRO
small**

www.small-journal.com

Figure 4. Raman results of O—H stretching vibration in a) 3 M $ZnSO_4$ and b) in situ gel; c) schematic diagram of the coordination state of zinc ions; d) schematic diagram of the hydrogen-bond network in different electrolytes; e) LSV results of zinc electrode with/without in situ hydrogel; CE profiles of Zn//Cu cell f) without and g) with in situ hydrogel.

cated by the large cluster of dendrites shown in Figure S15 (Supporting Information). Such dendrites have definitely followed the positive-feedback growth mode with considerable size increase in such short times. In contrast, the in situ hydrogel can effectively protect the zinc anode by suppressing dendrite growth. As previously mentioned, AM and MBAA get electrochemically polymerized on the zinc surface during electrochemical cycling. The symmetric cell with in situ hydrogel can safely operate for >5100 h at 0.5 mA cm^{-2} and 0.5 mAh cm^{-2}, which is 250 times longer than the control sample in the electrolyte (**Figure 5**a). The galvanostatic charge-discharge (GCD) profiles at different cycles show no evidence of decay, indicating the strong protection of the in situ hydrogel (Figure S16, Supporting Information). In comparison, the ex-situ gel presents far inferior performance of only 810 h, which can be attributed to the absence of self-adaptive ability (Figure S17, Supporting Information). Even at larger current densities, the lifespan of the symmetric cell with in situ hydrogel can be extended to 1800 h at 1 mA cm^{-2} and 1 mAh cm^{-2} (Figure S18, Supporting Information) and 1500 h at 5 mA cm^{-2} and 0.5 mAh cm^{-2} (Figure 5b), which is ≈30 times longer than that of traditional electrolytes. This performance is among the best using hydrogel as electrolytes (Figure 5c). The Zn—Zn symmetrical cell can operate normally at 60 °C (Figure S19, Supporting Information), indicating that in situ gel can take place at high temperatures. The polarization voltage of the cell at 60 °C is lower than that at 25 °C, since higher temperature leads to faster ion diffusion rates. Additionally, the rate performance of the zinc anode was studied using a fixed capacity of 0.5 mAh cm^{-2} and var-

ied current densities of 0.1, 0.2, 0.5, 1, 2, and 5 mA cm^{-2}. The cell with 3 M $ZnSO_4$ operated at current densities from 0.1 to 2 mA cm^{-2}, but failed at 5 mA cm^{-2}. It is widely accepted that high current densities deteriorate the lifespan of zinc anode by exacerbating the unbalanced distribution of the electric field, leading to the rapid growth of dendrite seeds generated at low current densities until failure.[26] In contrast, the cell with in situ gel displayed steady polarization at each current density, demonstrating the gel's excellent feasibility under rigorous conditions (Figure S20, Supporting Information). In addition, the hydrogel also guarantees a lower self-corrosion current rate and restricted 3D diffusion of ions, which is vital for metal anodes (Figures S21 and S22, Supporting Information).

It is reasonable to enquire the effectiveness of the hydrogel after the completion of the gelation process, and the morphology evolution of the zinc anode provides additional evidence. Impressively, the zinc deposition underneath the gel is regularly arranged in the form of hexagonal plates, which emerge after ten cycles (20 h) and overturn the original zinc surface (Figure 5d). After 500 cycles, the horizontally stacked hexagonal plates dominate the zinc surface (Figure 5e). Such preferential deposition is then verified by the X-ray diffraction (XRD) results. As shown in Figure 5f, bare zinc presents a typical profile of polycrystalline, in which (101) facets at $2\theta = 42.3°$ are the dominant arrangement. For the zinc anode protected by in situ hydrogel, the (002) facets at $2\theta = 36.3°$ dominate the structure, and the $I_{(002)/(101)}$ increases from 0.36 to 5.41 (20 h) and 6.29 (1000 h). Since the (002) facet owns the highest atomic packing density and lowest surface en-
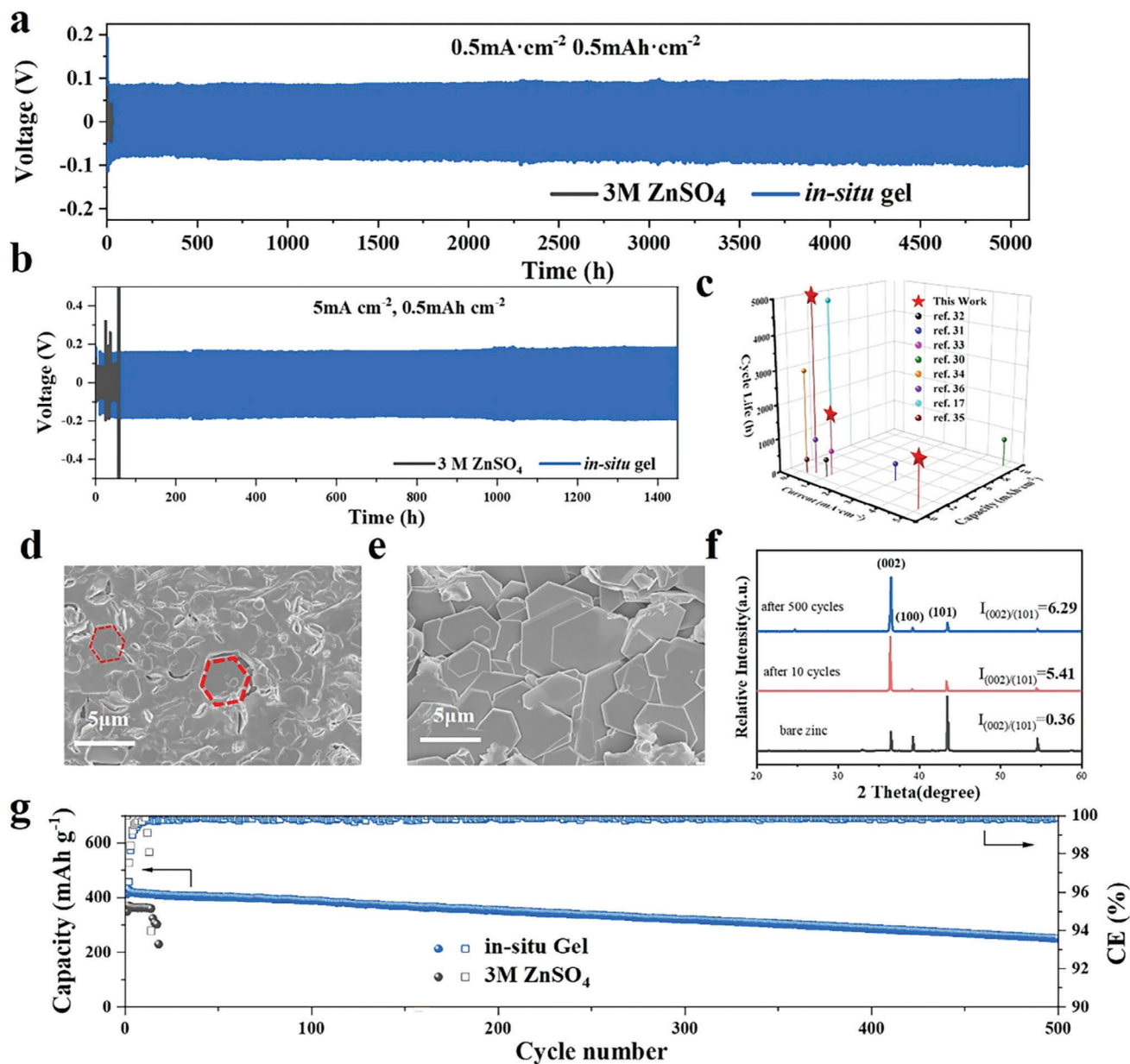
Figure 5. Electrochemical performance of in situ hydrogel. The long cycling performance of symmetric cells with in situ hydrogel at a) 0.5 Ma cm⁻² and b) 5 mA cm⁻²; c) comparison of cycling lifespan of symmetrical cells with hydrogel electrolyte in literature,[17,30–36] SEM image of the protected zinc anode after cycling for d) 20 h and e) 1000; f) XRD results of the zinc anode after different cycles; g) long cycling performance of ZnVO cathode at 0.5 A g⁻¹.

ergy, it is favorable for morphology control due to reversible epitaxial deposition.[4,27,28] Such highly oriented deposition is rational for dendrite suppression in the following cycles. We speculate the oriented deposition results from the confined diffusion of zinc ions in the hydrogel. The ultrafine porous structure exposes abundant acyl groups, which show high binding energy to zinc ions.[29] In the micro tunnels of the in situ gel, the zinc ions tend to coordinate with the acyl groups, which is verified by the dehydration of the solvation shell (Figure 4c). Our previous work confirms the zinc ions can be confined to the adjacencies of the functional groups and directionally diffuse along with the polymer chains.[12,15] leading to regular arrangement of the deposition. To sum up, the in situ hydrogel balances the electric field by its self-adaptive feature and directs the (002) facet-oriented deposition by functional groups. These two functions synergistically suppress the dendrite formation and prolong the lifetime of the zinc anode. This work opens a new avenue for orientation control through electrolyte tuning[28] rather than sophisticated substrate or coating materials.

To validate the effectiveness of the in situ hydrogel, zinc ion-based capacitors, and full batteries are assembled and investigated in coin cells. Active carbon (AC) is used as the cathode

material for the capacitor. As shown in Figure S23 (Supporting Information), the gel exhibits a close capacity release to the traditional electrolyte at each current density, indicating its applicability at various loads. Additionally, long-term cycling is conducted to study the stability of the zinc anodes. As illustrated in Figure S24 (Supporting Information), the cell with 3 M $ZnSO_4$ electrolyte operates for 835 cycles before experiencing a sudden potential drop, indicating a short circuit derived from dendrite at the anode side. In comparison, the cell with the protection of in situ gel can safely operate for more than 7500 cycles, >9 times longer than the traditional one. Furthermore, the zinc anode after 7000 cycles still presents a morphology of horizontally stacked hexagonal plates (Figure S25, Supporting Information), which explains the extended lifespan of the zinc anode and confirms the superior protective effect of the in situ gel. Note that a certain amount of hydrogel is required for dendrite suppression, and over thinning the gel would lead to inferior performance (Figure S26, Supporting Information). Moreover, $Zn_xV_2O_5$ (ZnVO) is synthesized as the cathode of the full battery following the literature.[37] The XRD result verifies the validity of the material (ICDD: 01-086-1238, Figure S27, Supporting Information). Then the transmission electron microscope images (Figure S28, Supporting Information) show the layer structure and nanosheet morphology, allowing for the conventional intercalation and de-intercalation of zinc ions. The CV curves of ZnVO in situ gel and 3 M $ZnSO_4$ electrolytes show similar profiles, guaranteeing the good electrochemical activity of ZnVO in the gel (Figure S29, Supporting Information). Later, the rate performance and long cycling performance of ZnVO in situ gel and 3 M $ZnSO_4$ electrolytes are tested. From Figure S30 (Supporting Information) it can be seen that ZnVO has similar rate performance in the two electrolytes, only showing slightly lower specific capacity at high current density (5 A g^{-1}) due to the increased polarization, as explained above. Figure 5g shows the excellent long-cycling performance of ZnVO in situ gel with 60.7% capacity retention after 500 cycles, while the ZnVO full cell in 3 M $ZnSO_4$ electrolytes experiences a quick short circuit after only 18 cycles. The results of the AC capacitor and ZnVO full cell demonstrate that the in situ gel can effectively prolong the battery's lifetime, proving its practical application prospects.

3. Conclusion

In summary, we have developed an electrochemically initiated and in situ hydrogel that is self-adaptive to the irregular configurations of the zinc metal due to the current-sensitive gelation process. The gel provides negative feedback to electric fields and ion flux concentration, promoting uniform stripping/plating reactions. The hydrogel's refined porous structure induces a preferred deposition of the (002) plane, which effectively suppresses dendrite formation. Additionally, the hydrogel reduces the activity of water in both free and coordination forms, which decreases HER tendencies and improves the reversibility of the zinc anode. As a result, the zinc anode exhibits an ultra-long lifespan of 5100 h at 0.5 mA cm^{-2} and 1500 h at 5 mA cm^{-2}, surpassing traditional electrolytes and ex situ gels by a significant margin. The in situ hydrogel is compatible with both the adsorption-type AC cathode and intercalation-type ZnVO cathode, resulting in enhanced stability of 7500 cycles (for AC) and 500 cycles (for

ZnVO) in full cells. This study provides an economical and efficient gelation approach that opens up new possibilities for the use of hydrogels in batteries.

Conflict of Interest

The authors declare no conflict of interest.

Data Availability Statement

The data that support the findings of this study are available from the corresponding author upon reasonable request.

[1] R. F. Service, *Science* **2021**, *372*, 890.
[2] G. Zampardi, F. La Mantia, *Nat. Commun.* **2022**, *13*, 687.
[3] P. Ruan, S. Liang, B. Lu, H. Fan, J. Zhou, *Angew. Chem., Int. Ed.* **2022**, *61*, e202200598.
[4] J. Zheng, Q. Zhao, T. Tang, J. Yin, C. D. Quilty, G. D. Renderos, X. Liu, Y. Deng, L. Wang, D. C. Bock, C. Jaye, D. Zhang, E. S. Takeuchi, K. J. Takeuchi, A. C. Marschilok, L. A. Archer, *Science* **2019**, *366*, 645.
[5] P. He, J. Huang, *ACS Energy Lett.* **2021**, *6*, 1990.
[6] R. Zhao, J. Yang, X. Han, Y. Wang, Q. Ni, Z. Hu, C. Wu, Y. Bai, *Adv. Energy Mater.* **2023**, *13*, 2203542.
[7] R. Qin, Y. Wang, L.u Yao, L. Yang, Q. Zhao, S. Ding, L. Liu, F. Pan, *Nano Energy* **2022**, *98*, 107333.
[8] T. Haxhimali, A. Karma, F. Gonzales, M. Rappaz, *Nat. Mater.* **2006**, *5*, 660.
[9] V. Fleury, *Nature* **1997**, *390*, 145.
[10] Y. Yang, H. Yang, R. Zhu, H. Zhou, *Energy Environ. Sci.* **2023**, *16*, 2723.
[11] Y. Cui, Q. Zhao, X. Wu, X. Chen, J. Yang, Y. Wang, R. Qin, S. Ding, Y. Song, J. Wu, K. Yang, Z. Wang, Z. Mei, Z. Song, H. Wu, Z. Jiang, G. Qian, L. Yang, F. Pan, *Angew. Chem., Int. Ed.* **2020**, *59*, 16594.
[12] Y. Wang, Y. Wang, C. Chen, X. Chen, Q. Zhao, L. Yang, L.u Yao, R. Qin, H. Wu, Z. Jiang, F. Pan, *Chem. Commun.* **2021**, *57*, 5326.
[13] R. Qin, Y. Wang, M. Zhang, Y. Wang, S. Ding, A. Song, H. Yi, L. Yang, Y. Song, Y. Cui, J. Liu, Z. Wang, S. Li, Q. Zhao, F. Pan, *Nano Energy* **2021**, *80*, 105478.

**ADVANCED
SCIENCE NEWS**

www.advancedsciencenews.com

**NANO · MICRO
small**

www.small-journal.com

[14] Y. Zhao, M. Ouyang, Y. Wang, R. Qin, H. Zhang, W. Pan, D. Y. C. Leung, B. Wu, X. Liu, N. P. Brandon, J. Xuan, F. Pan, H. Wang, *Adv. Funct. Mater.* **2022**, *32*, 2203019.

[15] L.u Yao, C. Hou, M. Liu, H. Chen, Q. Zhao, Y. Zhao, Y. Wang, L. Liu, Z.u-W. Yin, J. Qiu, S. Li, R. Qin, F. Pan, *Adv. Funct. Mater.* **2023**, *33*, 2209301.

[16] J. Wei, R. Li, L. Li, W. Wang, T. Chen, *Nano-Micro Lett.* **2022**, *14*, 182.

[17] Y. Qin, H. Li, C. Han, F. Mo, X. Wang, *Adv. Mater.* **2022**, *34*, 2207118.

[18] Y. Lu, C.-Z.i Zhao, J.-Q.i Huang, Q. Zhang, *Joule* **2022**, *6*, 1172.

[19] T. H. Wan, M. Saccoccio, C. Chen, F. Ciucci, *Electrochim. Acta* **2015**, *184*, 483.

[20] S. Ji, J. Qin, S. Yang, P. Shen, Y. Hu, K. Yang, H. Luo, J. Xu, *Energy Storage Mater.* **2023**, *55*, 236.

[21] S. Chen, P. Sun, J. Humphreys, P. Zou, M. Zhang, G. Jeerh, S. Tao, *Energy Storage Mater.* **2021**, *42*, 240.

[22] Y. Jiang, K. Ma, M. Sun, Y. Li, J. Liu, *Energy Environ. Mater.* **2023**, *6*, e12357.

[23] J. Zhou, L. Zhang, M. Peng, X.i Zhou, Y. Cao, J. Liu, X. Shen, C. Yan, T. Qian, *Adv. Mater.* **2022**, *34*, 2200131.

[24] A. Bayaguud, X. Luo, Y. Fu, C. Zhu, *ACS Energy Lett.* **2020**, *5*, 3012.

[25] J. Hao, B.o Li, X. Li, X. Zeng, S. Zhang, F. Yang, S. Liu, D. Li, C. Wu, Z. Guo, *Adv. Mater.* **2020**, *32*, 2003021.

[26] Q.i Yang, G. Liang, Y. Guo, Z. Liu, B. Yan, D. Wang, Z. Huang, X. Li, J. Fan, C. Zhi, *Adv. Mater.* **2019**, *31*, 1903778.

[27] S. D. Pu, C. Gong, Y. T. Tang, Z. Ning, J. Liu, S. Zhang, Y.i Yuan, D. Melvin, S. Yang, L. Pi, J.-J. Marie, B. Hu, M. Jenkins, Z. Li, B. Liu, S. C. E. Tsang, T. J. Marrow, R. C. Reed, X. Gao, P. G. Bruce, A. W. Robertson, *Adv. Mater.* **2022**, *34*, 2202552.

[28] W. Du, J. Yan, C. Cao, C. C. Li, *Energy Storage Mater.* **2022**, *52*, 329.

[29] Q.i Zhang, J. Luan, L. Fu, S. Wu, Y. Tang, X. Ji, H. Wang, *Angew. Chem., Int. Ed.* **2019**, *58*, 15841.

[30] H. Lu, J. Hu, L. Wang, J. Li, X. Ma, Z. Zhu, H. Li, Y. Zhao, Y. Li, J. Zhao, B. Xu, *Adv. Funct. Mater.* **2022**, *32*, 2112540.

[31] S. Huang, L. Hou, T. Li, Y. Jiao, P. Wu, *Adv Mater* **2022**, *34*, 2110140.

[32] W. Xu, C. Liu, S. Ren, D. Lee, J. Gwon, J. C. Flake, T. Lei, N. Baisakh, Q. Wu, *J. Mater. Chem. A* **2021**, *9*, 25651.

[33] W. Ling, F. Mo, J. Wang, Q. Liu, Y. Liu, Q. Yang, Y. Qiu, Y. Huang, M. T. Phys, **2021**, *20*, 100458.

[34] T. Wei, Y. Ren, Z. Li, X. Zhang, D. Ji, L. Hu, *Chem. Eng. J.* **2022**, *434*, 134646.

[35] C. Y. Chan, Z. Wang, Y. Li, H. Yu, B. Fei, J. H. Xin, *ACS Appl. Mater. Interfaces* **2021**, *13*, 30594.

[36] Y. Liu, H. He, A. Gao, J. Ling, F. Yi, J. Hao, Q. Li, D. Shu, *Chem. Eng. J.* **2022**, *446*, 137021.

[37] D. Kundu, B. D. Adams, V. Duffort, S. H. Vajargah, L. F. Nazar, *Nat. Energy* **2016**, *1*, 16119.